Journal of
Synchrotron
Radiation

ISSN 0909-0495

Received 29 February 2004
Accepted 5 January 2005

Two-wavelength MAD phasing and radiation damage: a case study

Ana González,[a] Frank von Delft,[b] Robert C. Liddington[c] and Constantina Bakolitsa[c]*

[a]Stanford Linear Accelerator Center, 2575 Sand Hill Road, Menlo Park, CA 94025, USA, [b]Syrrx Inc., 10410 Science Center Drive, San Diego, CA 92121, USA, and [c]The Burnham Institute, 10901 North Torrey Pines Road, La Jolla, CA 92037, USA. E-mail: bakolitsa@burnham.org

Radiation damage affects MAD experiments in two ways: (i) increased absorption by the crystal at the wavelengths of interest for the experiment results in faster crystal deterioration; (ii) lack of isomorphism induced by radiation damage causes problems when scaling and merging data at different wavelengths and can prevent accurate measurement of anomalous and dispersive differences. In an attempt to overcome these problems in the case of radiation-sensitive crystals of vinculin, two-wavelength MAD data were collected at the Se absorption-edge inflection and at high-energy remote wavelengths. Although this strategy resulted in a lower total absorbed dose compared with a standard three-wavelength experiment using the peak wavelength, an increase in the unit-cell volume and other effects attributable to radiation damage were still observed. In an effort to extract the maximum information available from the data, different data-processing and scaling procedures were compared. Scaling approaches involving local scaling of unmerged reflections were consistently successful and most ordered Se sites could be located. Subsequent use of these sites for phasing resulted in an interpretable electron density map. This case demonstrates the feasibility of two-wavelength MAD in the presence of moderate radiation damage using conventional data collection strategies and widely available standard software.

Keywords: two-wavelength MAD; radiation damage; vinculin.

1. Introduction

Although the problem of radiation damage appeared to have become largely manageable since the early 1990s through the development of cryo-techniques (reviewed by Garman & Schneider, 1997; Garman, 1999), it has re-emerged in recent years as a major concern during macromolecular crystallography experiments, particularly in the case of small or weakly diffracting crystals, which are becoming more frequently used particularly in intense third-generation synchrotron sources.

Specific effects of radiation damage on crystalline protein have been discussed, amongst others, by Ravelli & McSweeney (2000), Weik *et al.* (2002) and Burmeister (2000). They showed that radiation damage causes local changes in the protein structure, as well as small changes in orientation of the molecules and an increase of cell unit constant (Ravelli *et al.*, 2002). All these changes result in a lack of isomorphism that can complicate the scaling of diffracted intensities within and between data sets collected from the same crystal. This has particularly severe effects for structure solution based on anomalous dispersion methods: the small measured differences in diffracted intensities arising from anomalous dispersion can easily fall below the noise introduced by systematic loss of isomorphism and resolution during the experiment (Rice *et al.*, 2000), making structure solution difficult or impossible.

Careful measurement of the cell axes on organic crystals suggest that, at flux density levels typical for most macromolecular crystallography beamlines, non-specific damage to the sample increases linearly with the radiation dose absorbed by the crystal (Müller *et al.*, 2002), which can be approximated for an oscillation data set by the following expression,

$$\mathrm{Dose}_{\mathrm{total}} \simeq I\,[1 - \exp(-\eta z)]ENt, \qquad (1)$$

where I is the total beam photon flux in the crystal surface exposed to the beam; η is the linear absorption coefficient; z is the thickness of the crystal in the beam direction; E is the beam energy; N is the number of frames/degrees in the data set; and t is the exposure time per frame/degree.

Expression (1) implies that the intensity absorbed per second will be significantly increased during MAD and SAD experiments, and frequently on isomorphous replacement experiments; the increased absorbed intensity results from the

absorption coefficient η being about two order of magnitudes higher near absorption edges than at energies where photoelectric absorption can be neglected (see tables by Henke *et al.*, 1993). Even in samples with a relatively low ratio of anomalous scatterer to light atoms, the heavy atom contribution will be a large fraction of the total absorbed intensity. For example, the Se contribution at the Se *K*-edge peak wavelength is about 30% of the total absorption for a concentration corresponding to one Se atom per 1000 light atoms in the unit cell. At the chemical level, the increase in the absorbed dose translates to a higher number of ejected photoelectrons that will produce secondary ionization events, estimated at about 400 per 10 keV photoelectron (O'Neill *et al.*, 2002).

Because of the need to measure reflections at different wavelengths and separate measurements of Bijvoet or Friedel pairs, MAD and SAD phasing entail in general collecting reflections from a wider angle range and a larger number of frames N than required for a single set of unique reflections. This also contributes to increasing the total dose absorbed during the experiment.

The problem can be partially offset for such anomalous dispersion experiments by using shorter exposures per image; this applies particularly to good quality crystals diffracting to medium-high resolution (around 2.5 Å or better). In this case, data collection to the diffraction limit is not required for obtaining the structure by experimental phasing and the exposure time by frame could be decreased at least by half without seriously compromising structure solution. However, for poorly diffracting crystals, reducing the exposure time may not be an option. Although, as shown by Bass *et al.* (2002), phasing at resolutions lower than 4 Å can be carried out under favourable circumstances (abundant secondary helical structure, non-crystallographic symmetry, high solvent content *etc.*), higher resolution may be required in the general case for sufficient map interpretability.

Several proposals have been made to palliate the effects of radiation damage for phasing experiments using data from a single crystal and can be grouped under three main approaches: (i) to correct the reflection intensities for the damage at the data processing stage; (ii) to use radiation damage to obtain phase information; (iii) to attempt to minimize the radiation damage during data collection.

The first approach is illustrated by the 0-dose correction implemented by Diederichs *et al.* (2003). In general, this method has produced encouraging results, but appears to require a relatively high data redundancy to be stable. In addition, an adequate model for the radiation damage decay of the diffracted intensities fitting to all the cases has not yet been found. An advantage of attempting 0-dose correction is that it is, in principle, compatible with different data collection strategies and can be combined with the other approaches listed below.

The second approach postulates collection of highly redundant data at the peak wavelength (maximum absorption) and, if radiation damage occurs before the structure can be solved by SAD, uses radiation-damage-induced structure changes for phasing in a way analogous to isomorphous replacement. This is the RIP method, proposed by Ravelli *et al.* (2003).

The third approach seeks to minimize radiation damage effects to the phasing by using only the minimum amount of data required to solve the structure. González (2003) suggested that the optimal way to collect data for this purpose was to carry out a two-wavelength MAD experiment at the inflection and high-energy remote points. This approach was shown to require approximately the same amount of data [N in expression (1)] as the SAD approach, provided that a suitable remote wavelength far away from the edge was selected (González *et al.*, 1999). Because the absorption coefficient η at the remote and inflection wavelength decreases by roughly half with respect to the peak wavelength value, this strategy would result in a lower total dose absorbed by the experiment than the optimized SAD counterpart.

A potential problem with this data collection strategy is that it will not be able to totally eliminate noticeable radiation damage to the sample in every experiment. Thus, being able to deal with loss of isomorphism during the experiment will ultimately determine the feasibility of this approach in the general case.

Taking the precaution of collecting data 'simultaneously' at both wavelengths using φ wedges makes it easier to put the data on the same scale and extract the dispersive differences in the event of radiation damage. Data collection in wedges was, in fact, the standard approach to cope with radiation damage during MAD data collection before cryo-cooling techniques became commonplace (see reviews by Fourme & Hendrickson, 1990; Smith, 1991).

In this paper we will explore different alternatives to minimize the error introduced by radiation damage in the two-wavelength MAD experiment on vinculin crystals.

2. Vinculin structure solution

Vinculin is a 117 kDa highly conserved cytoskeletal protein with a critical involvement in cell adhesion and migration (Volberg *et al.*, 1995; Xu *et al.*, 1998; DeMali *et al.*, 2002). An intramolecular interaction controls access to the majority of ligands allowing vinculin to shuttle between the cytoplasm and the plasma membrane. Upon recruitment to cell–cell and cell–matrix adherens-type junctions, vinculin becomes activated and mediates a variety of protein–protein interactions that regulate the links between F-actin and the cadherin and integrin families of cell-adhesion molecules.

The crystal structure of full-length vinculin reveals an all α-helical architecture comprising eight four-helix bundles further organized into four tandem pairs. The structure shows the autoinhibited conformation of vinculin in which the C-terminal tail domain is held pincer-like by the vinculin head, and ligand binding is regulated both sterically and allosterically. This organization allows for a combinatorial output to different input signals and ensures that vinculin is activated only at sites of cell adhesion when two or more of its binding partners are brought into apposition (Bakolitsa *et al.*, 2004). The atomic coordinates have been deposited in the Protein

Data Bank under accession codes 1ST6 (coordinates) and r1ST6sf (structure factors).

2.1. Data collection

Vinculin could be crystallized in three different space groups ($C2$, $P2_1$, $C222_1$), all of which were problematic. All crystal forms grew predominantly as clusters of thin plates and, whereas $C2$ crystals were rarely obtained, $P2_1$ and $C222_1$ crystals both had a long (>350 Å) cell axis along the thinnest plate dimension (b^* and c^*, respectively). In the flat cryoloop, the long cell axis was therefore always oriented perpendicular to the mounting pin axis which, in combination with a large mosaic spread (typically 1°, 0.5° for the best crystals), led to unacceptable reflection overlap and thus data incompleteness, unless the κ-axis was offset by 45° in order to avoid the long cell axis being perpendicular to the oscillation axis.

In addition, all crystal forms were found to be sensitive to radiation damage, particularly Se-MET crystals. Vinculin has 39 seleno-methionine residues and is thus strongly absorbing at 0.98 Å and shorter wavelengths near the absorption edge (the absorbed dose for the Se-MET form is between 2.5 and 1.8 times larger than for the native at the same wavelengths). On SSRL wiggler beamlines, with intensities typical for second-generation beamlines ($\sim 10^{12}$ photons s^{-1} mm^{-2}), the Se-MET-containing crystals were damaged after about 15 h in the beam (5 min per degree) at the Se 'peak' (absorption-edge white line) wavelength, for an absorbed dose about one order of magnitude less than the Henderson limit of 2×10^7 Gy (Henderson, 1990). The long exposure times were needed because of the weak diffraction from these crystals. These data could not be used to obtain any useful structural information, most likely because of the combination of poor diffraction (the maximum resolution was 3.8 Å) and radiation damage.

The radiation decay in this preliminary experiment suggested that a three-wavelength MAD experiment at the peak, inflection and remote wavelengths was unlikely to be successful, even using the orthorhombic form [in principle requiring only 90° per wavelength to collect a complete data set including Bijvoet pairs (Dauter, 1997)]. Owing to the κ offset required by the crystal morphology, a number of other data collection strategies (mirror, inverse beam) could not be considered, while an inaccessible zone of $\sim$80° with the above-mentioned κ offset made redundancy for the $P2_1$ crystal form problematic. Thus it was anticipated that a SAD experiment would be difficult in this case.

In order to extend the lifetime of the crystal long enough to be able to collect enough data for structure solution, MAD data collection was carried out on the orthorhombic crystal form at the Se K-edge inflection and remote wavelengths (0.979 and 0.94 Å, respectively), alternating in 10° wedges at each wavelength to be able to preserve the dispersive differences in the event of radiation damage. A total of 110° were collected at each wavelength. The dose per second at the two wavelengths used for the data collection is estimated at 24 and 18 Gy, which amounts to a total dose absorbed during the experiment of between 5×10^5 and 6×10^5 Gy. The estimates

Table 1
Merging statistics (from *SCALA*) for the remote and inflection wavelength data.

R-merge: $\Sigma|I - \langle I\rangle|/\Sigma I$; R-meas: redundancy-independent (multiplicity-weighted) R-merge (Diederichs & Karplus, 1997); R-anom: $\Sigma|\langle I^+\rangle - \langle I^-\rangle|/\Sigma(\langle I^+\rangle + \langle I^-\rangle)$.

	Remote wavelength	Inflection wavelength
R-merge	0.09	0.1
R-meas	0.11	0.13
R-anom	0.06	0.08
$\langle I\rangle/\sigma I$	13.1	11.9
N-unique	26278	26279
Completeness	100%	100%
Anom-completeness	100%	99.8%
Multiplicity	4.4	4.4

for the anomalous scattering factors f' and f'' were obtained from a fluorescence scan of the sample using a modified version of the program *CHOOCH* (Evans & Pettifer, 2001; McPhillips *et al.*, 2002). For this pair of wavelengths, $\Delta f'$ was 10.8 electrons and f'' was 4.5 and 3.5 electrons at the inflection and remote wavelengths, respectively, resulting in very high theoretical fractional anomalous and dispersive differences (above 10% of the total structure factor amplitude).

The data used for structure determination were collected at the SSRL beamline 9-1 on a 245 mm MAR research image-plate detector, using the program *Blu-ice* (McPhillips *et al.*, 2002). The exposure time was approximately 2 min per degree and dose-corrected ('dose mode') to compensate for the X-ray beam intensity decay during the experiment, evaluated from the readings of an ion chamber detector. The dose correction was also used to compensate for the slightly lower intensity at the remote wavelength, since both the ion chamber signal and diffracted intensity vary with the wavelength approximately as λ^2. Data were collected to 3.2 Å. The overall statistics for the two data sets are shown in Table 1. The R-factors (plotted as a function of resolution in Fig. 1) and $I/\sigma I$ are slightly better for the remote-wavelength data. This may mean that the dose exposure time was slightly over-corrected at the remote wavelength, perhaps because of additional differences in the ion chamber response caused by the read-out electronics.

Data integration and scaling was carried out using *DENZO*/*SCALEPACK* (Otwinowski & Minor, 1997), *MOSFLM* (Leslie, 1991; Collaborative Computational Project, Number 4, 1994) and *SCALA* (Collaborative Computational Project, Number 4, 1994). Although the R-merge residuals from different programs varied (see Fig. 1), the Se substructure, and ultimately the entire structure, could be solved by processing and scaling the data with either program.

2.2. Solving the Se atom substructure and phasing

The ordered Se sites could be successfully solved by combining all the unmerged reflections measured at both wavelengths for scaling and calculation of the anomalous component of the structure factor FA. The FA component could be calculated using either *XPREP* or *SHELXC* (Sheldrick, 2003), after previous scaling with *SCALA* or *SCALE-*

Table 2
R_{cullis} values for experimental phasing (with *SHARP*) and results from automated model building after density modification with *RESOLVE* (Terwilliger, 2003), with data subjected to different scaling protocols.

Scaling protocols: 0-dose, the radiation-damage correction algorithm implemented by Diederichs & Karplus (1997) was applied to the data before scaling with *XSCALE* (Kabsch, 1988); *SCALA* (local), the scales for each data set were calculated following the procedure suggested by Evans (1997) to improve MAD data. The data sets scaled with *SCALA* (local and simple scaling) were also scaled together with *SCALEIT* prior to phasing. In the case of simple scaling with *SCALA*, the statistics using only 80% complete data sets at each wavelength are also shown (the Se substructure could not be solved with lower completeness).

				SCALA	
	0-dose + *XSCALE*	*SCALEPACK*	*SCALA* (local)	All data	80% complete
R_{cullis} Anom (remote)	0.91	0.84	0.86	0.81	0.82
R_{cullis} Anom (inflection)	0.85	0.78	0.81	0.75	0.77
R_{cullis} Disp (acentric)	0.91	0.81	0.68	0.65	0.67
R_{cullis} Disp (centric)	0.88	0.85	0.74	0.60	0.73
No. of main chain residues built	600	924	802	804	648
No. of disconnected fragments	66	113	82	82	64

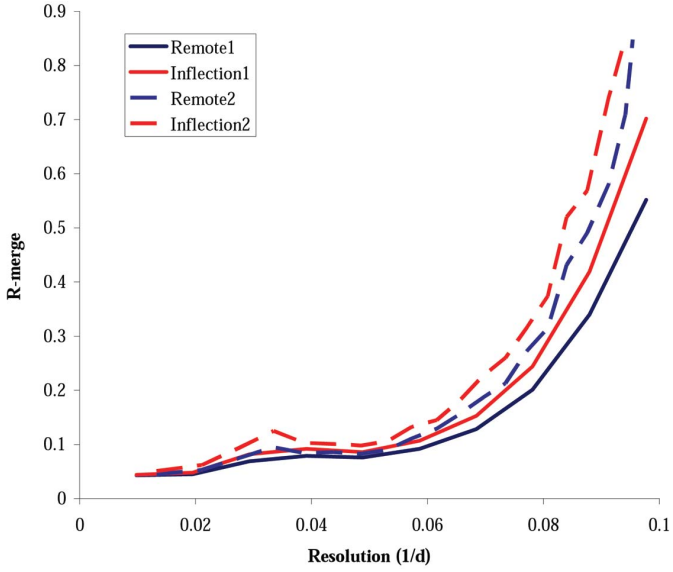

Figure 1
R-merge as a function of resolution for the two-wavelength data sets. The continuous line and dashed line plots were obtained by scaling the data using *SCALA* and *SCALEPACK*, respectively.

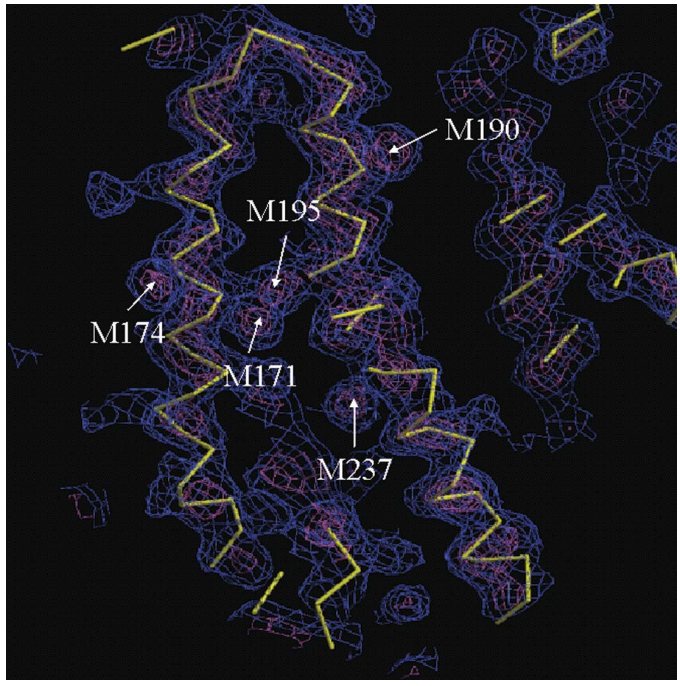

Figure 2
A 4 Å experimental electron density map with the C-α backbone trace in yellow. The blue and pink density correspond to 1σ and 3σ contour levels, respectively. Density for selenium sites and corresponding residues are indicated by arrows.

PACK. The correct substructure solution could be found subsequently using the program *SHELXD* (Schneider & Sheldrick, 2002). Correct solutions were easily distinguished from incorrect ones by the large difference in the correlation factor (over 0.4 for the correct compared with 0.2–0.25 for the incorrect solutions). The correct hand could be determined easily using the program *SHELXE* (Sheldrick, 2002).

Determining whether all the sites in a given solution were correct was more laborious, as there was no clear occupancy drop for the sites. The surest way to determine this was to refine the sites during phasing using *SHARP* (de La Fortelle *et al.*, 1997). The coordinates and occupancy were refined, but not the temperature factors. Using this approach, 25 to 27 of the top Se sites were deemed correct (two of the lowest-occupancy sites could be refined or not depending on how the data were processed). Using these sites, it was always possible to obtain an interpretable map (Fig. 2), even when using other software for phasing. The experimental phasing statistics and automated model building results obtained using *RESOLVE* (Terwilliger, 2003) are shown in Table 2.

2.3. Dose correction

A different approach to the structure solution consisted of applying the 0-dose correction implemented by Diederichs *et al.* (2003) to the remote and inflection wavelength data sets. Decay factors were calculated and corresponding weights applied every 10° in accordance with the data collection procedure. With this correction, the anomalous signal increased significantly for both wavelengths (see Table 3.) This improvement was not sufficient to be able to solve the substructure by SAD with either wavelength. Structure solution by MAD could be performed following the same scaling

Table 3
Increase in the anomalous signal applying the 0-dose correction.

The anomalous signal here is defined as the ratio between the mean value of $\sigma(I)$ for acentric reflections assuming Friedel pairs are symmetry equivalents and the mean value of $\sigma(I)$ for acentric reflections keeping Friedel pairs separate.

	All reflections	$I > 2\sigma$	$I > 4\sigma$	$I > 6\sigma$
Remote wavelength				
Anomalous signal (uncorrected)	1.11	1.13	1.15	1.16
Anomalous signal (corrected)	1.19	1.25	1.28	1.29
Inflection wavelength				
Anomalous signal (uncorrected)	1.19	1.26	1.29	1.27
Anomalous signal (corrected)	1.26	1.36	1.40	1.38

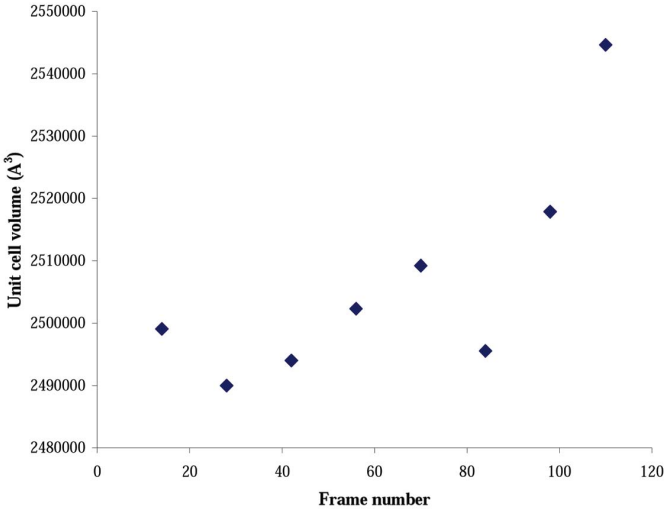

Figure 3
Increase of the cell volume during data collection (based on post-refinement of the unit-cell dimensions in blocks of ten frames).

and phasing procedure described in §2.1. The phasing results are shown in Table 2.

3. Discussion

3.1. Effects of radiation damage during data collection

Although the estimated dose received by the crystal in this experiment was about half of that which had previously been observed to cause damage to the crystals, these data also showed some evidence of radiation damage during the experiment. A total increase in the unit-cell volume of 1.6% was observed (see Fig. 3). This is consistent with previously reported values for the expansion in the unit cell (Murray & Garman, 2002). The mosaicity also increased during data collection (Fig. 4). The *R*-merge values, on the other hand, did not show a steady increase as a function of frame (Fig. 5).

Localized radiation damage to the Se sites might in principle be observed by calculating Fourier difference maps between the beginning and the end of the data collection. Dispersive difference maps using the first and second half of the data were compared. The completeness of the two data halves (around 76 and 72%, respectively) were high enough to

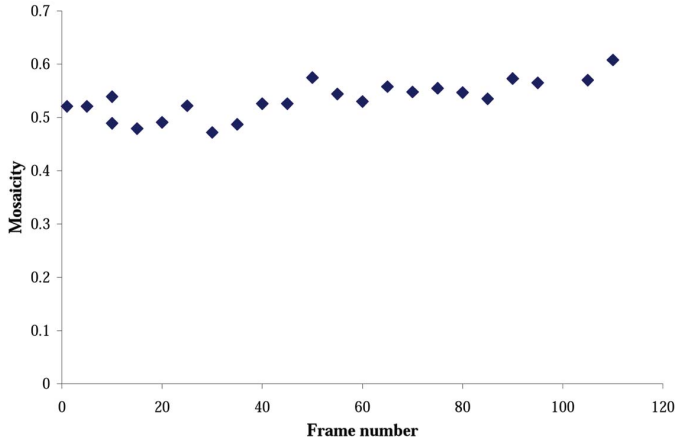

Figure 4
Mosaic spread as a function of frame number (the value for every fifth frame is plotted).

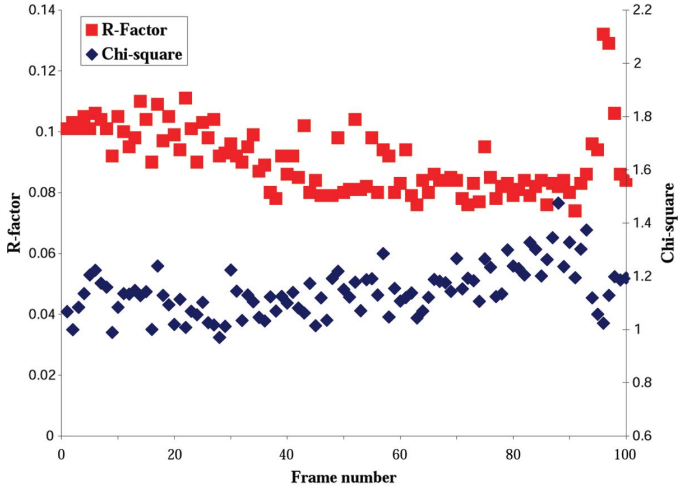

Figure 5
R-factor and χ^2 values as a function of frame number.

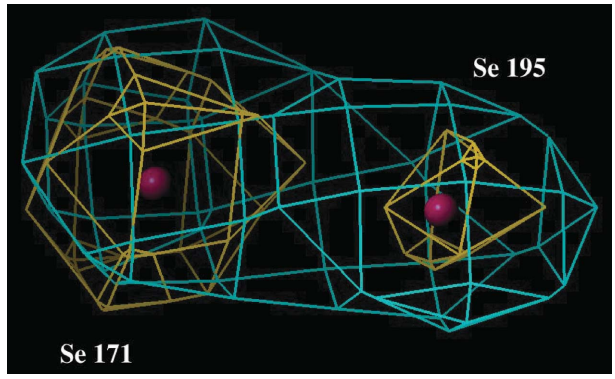

Figure 6
Phased-dispersive difference Fourier maps around two Se sites calculated with the first (blue) and second (coral) halves of the MAD data and contoured at the 6σ level. The Se atoms are 4.4 Å apart. The electron density peaks are of similar height for site 171 (about 14σ), which suggests that it is not affected by radiation damage. For site 195, the second half-peak is slightly lower (8σ compared with 12σ for the peak for the first half of the data). This may be an indication that this site is affected by radiation.

obtain clear peaks corresponding to the Se sites. The anomalous differences were, however, very noisy, probably owing to the low percentage of anomalous differences contained in the truncated data sets.

Proximity of selenium sites to one another does appear to exacerbate radiation damage for one or more of the neighbours. Based on the dispersive differences, one site (corresponding to Se-MET 195) showed a large decrease in peak height for the second half of the experiment, whereas the neighbouring site (Se-MET 171), 4.4 Å away, was apparently unaffected (Fig. 6). The proximity of Se-MET 171 to C138, only 3.3 Å away in the model, might explain this differential sensitivity, since C138 could act as a free-radical scavenging residue. More data at a higher accumulated dose would be required to confirm that Se-MET 195 is indeed particularly sensitive to radiation damage. Se-MET 930 provides further circumstantial evidence for the effect of damage by proximity to another anomalous scatterer: although all other buried Se sites were located before phasing, this site was not, even though it is buried too. This site is close to the Se atoms of M933 (at a distance of 4.1 Å), M898 (4.2 Å) and M1031 (4.6 Å), which would result in a very high concentration of photoelectrons at its position. The Se-MET 933 is, in turn, close to Cys 950 (5 Å). (See also supplemental data.[1])

3.2. Optimal treatment of data

The data sets showed a strong anomalous signal correlation at low resolution (see Fig. 7). This is to be expected, as the ratio of anomalous scatterers to light atoms was high. Despite the high anomalous signal, many attempts to solve the Se substructure after scaling and merging the data separately failed. Keeping the reflections unmerged during scaling appeared to be a crucial step to finding the correct solution. The only instance where a substructure solution containing 18 correct sites could be located with merged data was after using the scaling procedure (with *SCALA*) proposed by Evans (1997), namely 'local' scaling of both wavelengths individually to a reference data set created independently by scaling and merging the two wavelengths together, and then calculating the FAs using *XPREP*. Even in this case it took over 200 attempts to find the marginal solution. In contrast, following the same procedure but using unmerged reflections to calculate the FAs, all the correct sites were found in less than 20 attempts. This implies that merging the reflections at an early stage of the structure solution is counterproductive in difficult cases.

Although the 0-dose data correction implemented by Diederichs *et al.* (2003) resulted in an improvement in the anomalous (Bijvoet) differences, the phases were not improved. This correction procedure has been shown to work well with redundant data (eightfold multiplicity). In the case of the vinculin data, however, the lower value of the multiplicity (4.4) may have resulted in overfitting of the correcting parameters.

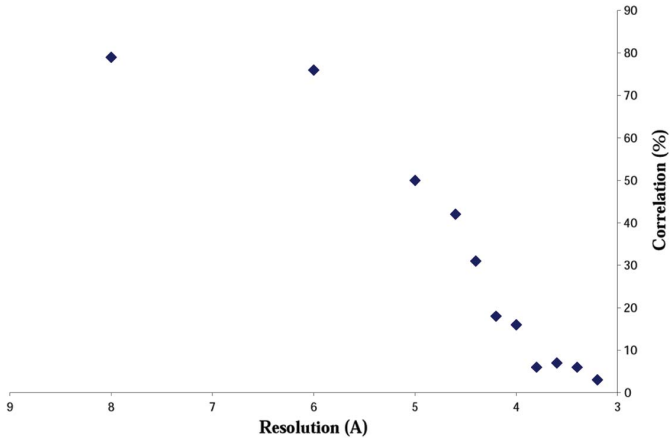

Figure 7
Anomalous difference correlation between the inflection and remote wavelength data (from *SHELXC*). Based on these values, there is a significant anomalous signal at 4.3 Å and lower resolutions.

Despite the sizable dispersive and anomalous contributions to the MAD data set, attempting to derive the sites from anomalous or dispersive differences alone was not successful, no matter what scaling protocol was applied to the data. Both sources had to be combined.

3.3. Refining the data collection strategy

It was established that substructure solution was still possible using as few as 67° of the collected data at each wavelength, corresponding to a unique completeness of about 80% and acentric pair completeness of 70% for each wavelength. The phasing statistics obtained with this incomplete MAD data set (displayed in Table 2) imply that there is not a great deal of improvement in the individual experimental phases by collecting more data. However, the performance of density modification is better with higher completeness: using a complete data set for density modification and model building after phasing with 80% of the data allows tracing an additional 15% of the main chain.

Being able to solve the structure with incomplete MAD data sets is not unusual, as pointed out by González (2003). Thus it may have been possible to refine further the data collection strategy for radiation-sensitive crystals by aiming for a data completeness of, for example, 90% (this should be safe for cases with a high predicted anomalous signal) and employing the remaining lifetime of the crystal for collection of complete and more redundant data at a single wavelength. This data collection strategy could be an advantage in cases such as this, where good quality crystals are rare and the data collected for structure solution must also be used for refining the resultant model.

4. Conclusions

The results presented above show that two-wavelength MAD data collection at the inflection and a high-energy remote

[1] Supplementary data for this paper are available from the IUCr electronic archives (Reference: XN0002). Services for accessing these data are described at the back of the journal.

wavelength can be a suitable strategy to solve the structure even for difficult cases. Although the two-wavelength strategy did not totally prevent radiation damage to the sample during the experiment, the effects in the data and the structure are very slight at the resolution the data were collected. The data collection in wedges may have also contributed to preserving the signal and facilitating structure solution.

A SAD experiment carried out at the peak of the absorption-edge white line would have resulted in an absorbed dose per second of 39 Gy, *i.e.* almost double the rate than in the two-wavelength MAD experiment. Even if the structure could have been solved by optimized SAD using half as much data as in the MAD case [which is not common, according to the results obtained by González (2003)], there would not have been a big advantage in using SAD in terms of decreased radiation damage. Because of the difficulties in collecting redundant SAD data for one of these crystals (which even with damage could have been rescued with a suitable correction for radiation decay of the intensities or else used for RIP phasing), it can be concluded that two-wavelength MAD was the optimal strategy in this particular case[2].

Local scaling of the unmerged intensities and combining anomalous and dispersive differences to calculate the anomalous scatterer substructure were critical for the success of the experiment.

This experiment did not allow a direct comparison between the performance of two-wavelength MAD *versus* SAD. More experiments are required to determine the best data collection strategy in a more general case.

Portions of this research were carried out at the Stanford Synchrotron Radiation Laboratory, a national user facility operated by Stanford University on behalf of the US Department of Energy, Office of Basic Energy Sciences. The SSRL Structural Molecular Biology Program is supported by the Department of Energy, Office of Biological and Environmental Research, and by the National Institutes of Health, National Center for Research Resources, Biomedical Technology Program, and the National Institute of General Medical Sciences.

References

Bakolitsa, C., Cohen, D. M., Bankston, L. A., Bobkov, A. A., Cadwell, G. W., Jennings, L., Critchley, D. R., Craig, S. W. & Liddington R. C. (2004). *Nature (London)*, **430**, 583–586.

Bass, B. R., Strop, P., Barclay, M. & Rees, D. C. (2002). *Science*, **298**, 1582–1587.

[2] Since the two-wavelength MAD experiment described here was carried out, the structure of full-length vinculin solved by SAD at the Se absorption edge peak has also been published by Borgon *et al.* (2004). In this work, seven crystals were used to overcome the radiation damage during phasing. The crystals used for this experiment diffracted to higher resolution (2.85 Å), and the longest unit-cell axis was approximately 153 Å; in addition, the phases could be improved with twofold non-crystalline symmetry averaging and a molecular replacement model existed for about 50% of the scattering mass. The SAD maps obtained were nevertheless reported to be challenging. It is not known if RIP or a 0-dose correction was attempted for these data.

Borgon, R. A., Vonrhein, C., Bricogne, G., Bois, P. R. & Izard, T. (2004). *Structure*, **12**, 1189–1197.

Burmeister, W. P. (2000). *Acta Cryst.* D**56**, 328–341.

Collaborative Computational Project, Number 4 (1994). *Acta Cryst.* D**50**, 760–763.

Dauter, Z. (1997). *Methods Enzymol.* **276**, 326–344.

DeMali, K. A., Barlow, C. A. & Burridge, K. (2002). *J. Cell Biol.* **159**, 881–891.

Evans, P. R. (1997). *Proceedings of the CCP4 Study Weekend on Recent Advances in Phasing*, pp. 97–102, edited by K. S. Wilson, G. Davies, A. W. Ashton and S. Bailey. Warrington: CCLRC Daresbury Laboratory.

Diederichs, K. & Karplus, P. A. (1997). *Nature Struct. Biol.* **4**, 269–275.

Diederichs, K., McSweeney, S. & Ravelli, R. B. G. (2003). *Acta Cryst.* D**59**, 903–909.

Evans, G. & Pettifer, R. F. (2001). *J. Appl. Cryst.* **34**, 82–86.

Fourme, R. & Hendrickson, W. A. (1990). *Synchrotron Radiation and Biophysics*, edited by S. S. Hasnain, pp. 156–175. Chichester: Horwood.

Garman, E. (1999). *Acta Cryst.* D**55**, 1641–1653.

Garman, E. F. & Schneider, T. R. (1997). *J. Appl. Cryst.* **30**, 211–237.

González, A. (2003). *Acta Cryst.* D**59**, 315–322.

González, A., Pédelacq, J.-D., Solà, M., Gomis-Rüth, F. X., Collect, M., Samama, J.-P. & Benini, S. (1999). *Acta Cryst.* D**55**, 1449–1458.

Henderson, R. (1990). *Proc. R. Soc. London Ser. B*, **241**, 6–8.

Henke, B. L., Gullikson, E. M. & Davis, J. C. (1993). *Atom. Data Nucl. Data Tables*, **54**, 181–342.

Kabsch, W. (1988). *J. Appl. Cryst.* **21**, 916–924.

La Fortelle, E. de, Irwin, J. J. & Bricogne, G. (1997). In *Crystallographic Computing 7*, edited by Philip Bourne and Keith Watenpaugh. Oxford University Press.

Leslie, A. G. W. (1991). *Crystallographic Computing V*, edited by D. Moras, A. D. Podjarny and J. C. Thierry, pp. 27–38. Oxford University Press.

McPhillips, T. M., McPhillips, S. E., Chiu, H.-J., Cohen, A. E., Deacon, A. M., Ellis, P., Garman, E., González, A., Sauter, N. K., Phizackerley, R. P., Soltis, S. M. & Kuhn, P. (2002). *J. Synchrotron Rad.* **9**, 401–406.

Müller, R., Weckert, E., Zellner, J. & Drakopoulos, M. (2002). *J. Synchrotron Rad.* **9**, 368–374.

Murray, J. M. & Garman, E. F. (2002). *J. Synchrotron Rad.* **9**, 347–354.

O'Neill, P., Stevens, D. L. & Garman, E. F. (2002). *J. Synchrotron Rad.* **9**, 329–332.

Otwinowski, Z. & Minor, W. (1997). *Methods Enzymol.* **276**, 307–326.

Ravelli, R. B. G. & McSweeney, S. (2000). *Structure*, **8**, 315–328.

Ravelli, R. B. G., Schrøder Leiros, H.-K., Pan, B., Caffrey, M. & McSweeney, S. (2003). *Structure*, **11**, 217–224.

Ravelli, R. B. G., Theveneau, P., McSweeney, S. & Caffrey, M. (2002). *J. Synchrotron Rad.* **9**, 355–360.

Rice, L. M., Earnest, T. N. & Brünger, A. T. (2000). *Acta Cryst.* D**56**, 1413–1420.

Schneider, T. R. & Sheldrick, G. M. (2002). *Acta Cryst.* D**58**, 1772–1779.

Sheldrick, G. M. (2002). *Z. Kristallogr.* **217**, 644–650.

Sheldrick, G. M. (2003). *SHELXC*. University of Göttingen, Germany.

Smith, J. L. (1991). *Curr. Opin. Struct. Biol.* **1**, 1002–1011.

Terwilliger, T. C. (2003). *Acta Cryst.* D**59**, 1174–1182.

Volberg, T., Geiger, B., Kam, Z., Pankov, R., Simcha, I., Sabanay, H., Collect, J. L., Adamson, E. & Ben-Ze'ev, A. (1995). *J. Cell Sci.* **108**, 2253–2260.

Weik, M., Bergès, J., Raves, M. L., Gros, P., McSweeney, S., Silman, I., Sussman, J. L., Houée-Levin, C. & Ravelli, R. B. G. (2002). *J. Synchrotron Rad.* **9**, 342–346.

Xu, W., Baribault, H. & Adamson, E. D. (1998). *Development*, **125**, 327–337.